

Supplementary Information

Cutoff-Voltage-Dependent Low-Voltage Structural Evolution and Apparent Capacity Balancing in Spinel $\text{LiFe}_{0.5}\text{Mn}_{1.5}\text{O}_4$

Zuojun Yang^a, Shun Zheng^a, Guokang Chen^a, Qinfeng Zheng^a, Xuheng Jiang^a, Chenji Hu^a, Pengtao Xu^a, Yixiao Zhang^{a, *}, Xi Liu^{a, b, c, *}, Liwei Chen^{a, b, *}

^a School of Chemistry and Chemical Engineering, in-situ Center for Physical Sciences, Shanghai Electrochemical Energy Device Research Center (SEED), Shanghai Jiao Tong University, Shanghai 200240, P.R. China

^b Frontiers Science Center for Transformative Molecules, Shanghai Jiao Tong University, Shanghai 200240, P. R. China

^c School of Chemistry and Chemical Engineering, Ningxia University, Yinchuan 750021, P.R. China

Corresponding authors:

E-mail: yxzhang2019@sjtu.edu.cn, liuxi@sjtu.edu.cn, lwchen2018@sjtu.edu.cn.

Experimental section

Synthesis of LFMO. Spinel LFMO was synthesized via a conventional high-temperature solid-state reaction. Li_2CO_3 (Aladdin, 99%), MnO_2 (Alfa Aesar, 99.9%), and Fe_2O_3 (Alfa Aesar, 99.9%) were used as starting materials. To compensate for lithium loss during high-temperature calcination, 5% excess Li_2CO_3 was added. The precursors were mixed in ethanol using a planetary ball mill, followed by vacuum drying at 60 °C for 12 h. The dried powders were pressed into pellets and calcined at 850 °C for 18 h in air. After natural cooling to room temperature, the pellets were ground into fine powders for subsequent characterization and electrode fabrication.

Electrode preparation and electrochemical measurements. Cathodes were prepared by mixing 70 wt% LFMO, 20 wt% Super C65 conductive carbon (Timcal), and 10 wt% poly(vinylidene fluoride) (PVDF, Solvay 5130) in N-methyl-2-pyrrolidone (NMP, Aladdin, 99.9%) to form a homogeneous slurry. The resulting slurry was cast onto aluminum foil using a doctor blade with a gap of 200 μm , followed by drying under vacuum at 100 °C overnight. The dried electrodes were punched into 12 mm diameter disks, with an average active-material loading of $\sim 1.0 \text{ mg cm}^{-2}$. CR2025 coin-type half-cells were assembled in an Ar-filled glovebox using lithium metal foil as the counter/reference electrode, Celgard 2400 as the separator, and a high-voltage electrolyte (LB-372, DoDoChem). Galvanostatic charge–discharge measurements were conducted on a Neware battery testing system (CT-4800T) at 30 °C over voltage windows of 5.2–1.5 V and 5.2–2.5 V. Differential capacity (dQ/dV) curves were obtained by numerical differentiation of the galvanostatic profiles. All data analysis and

plotting were performed using Origin.

Ex situ XRD and Rietveld refinement. Powder X-ray diffraction (XRD) patterns were collected on a Bruker D8 Advance diffractometer using Cu $K\alpha$ radiation ($\lambda=1.54178 \text{ \AA}$) in reflection geometry. Data were recorded with a 2θ step size of 0.02° and a counting time of 0.2 s per step. Rietveld refinements were performed using Topas (version 6) software. For discharged samples showing phase coexistence, a two-phase model consisting of a cubic spinel phase ($Fd\bar{3}m$) and a tetragonal phase ($I4_1$) was employed. The crystallographic models were obtained from the Crystallography Open Database (COD).

Operando XRD. Operando XRD measurements were performed on a Bruker D8 Advance diffractometer with Cu $K\alpha$ radiation in reflection geometry. A custom-designed electrochemical cell equipped with a Be window was used to enable real-time diffraction during electrochemical cycling. The working electrode was prepared using the same composition as the coin-cell electrodes (70 wt% LFMO, 20 wt% Super C65, 10 wt% PVDF). The slurry was coated onto Al foil and dried under vacuum at 100°C overnight, yielding an active-material loading of $\sim 2 \text{ mg cm}^{-2}$. The electrolyte was LB-372 (DoDoChem), and a Celgard separator was used. The cell was cycled using a Neware battery testing system (CT-4800T), and XRD patterns were continuously collected with a scan time of approximately 10 min per pattern during the first charge–discharge process.

X-ray absorption spectroscopy. Mn and Fe K -edge X-ray absorption spectroscopy (XAS) was carried out at the Shanghai Synchrotron Radiation Facility

(SSRF, BL14W) in fluorescence mode. Electrodes were harvested at the pristine state and after discharge to 3.5, 2.5, and 1.5 V (denoted as D3.5 V, D2.5 V, and D1.5 V, respectively) for X-ray absorption near-edge structure (XANES) analysis. XANES spectra were processed using the Athena software package and normalized to an intensity range of 0–1 prior to analysis.

Electron microscopy. Morphologies were examined by scanning electron microscopy (SEM, Hitachi SU8240/Regulus series). Elemental distributions were analyzed by energy-dispersive X-ray spectroscopy (EDS). Atomic-resolution structural characterization was performed using aberration-corrected scanning transmission electron microscopy (AC-STEM, Hitachi HF5000) equipped with a high-angle annular dark-field (HAADF) detector. For ex situ TEM/STEM observations, cells were disassembled in an Ar-filled glovebox; the electrodes were rinsed with dimethyl carbonate (DMC) to remove residual electrolyte, dried, and the scraped powders were dispersed in anhydrous ethanol and drop-cast onto Cu grids.

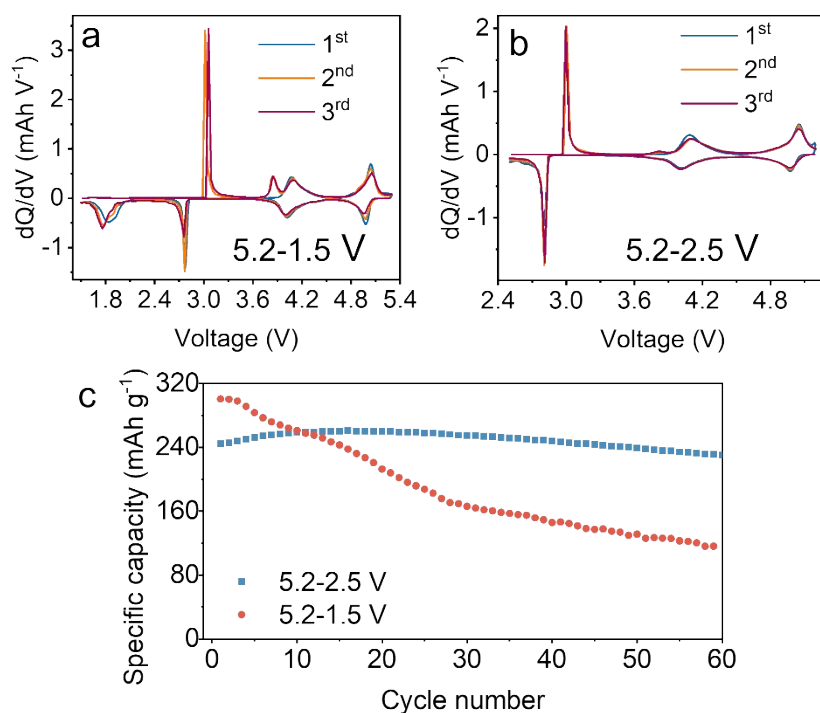


Fig. S1 Differential capacity (dQ/dV) curves for the first three cycles in the (a) 5.2–1.5 V and (b) 5.2–2.5 V windows. (c) Cycling performances in the 5.2–1.5 V and 5.2–2.5 V windows.

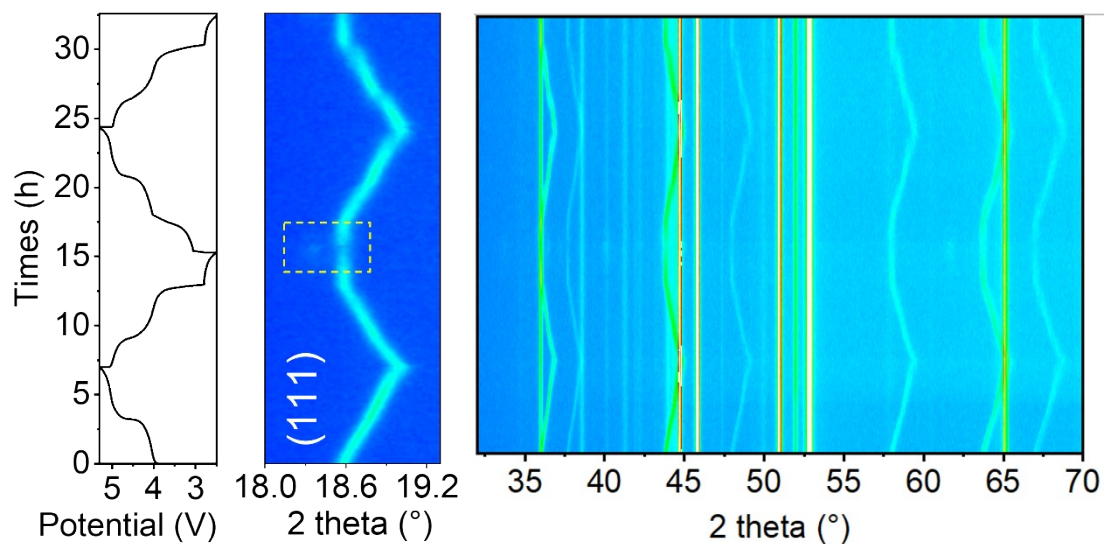


Fig. S2 Operando XRD test in 5.2-2.5 V windows.

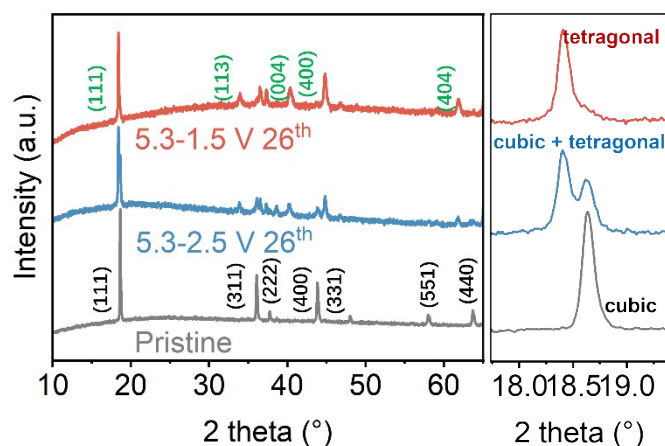


Fig. S3 Ex-situ XRD patterns of pristine LFMO, and the electrodes cycled within 5.2–2.5 V and 5.2–1.5 V for 26 cycles.

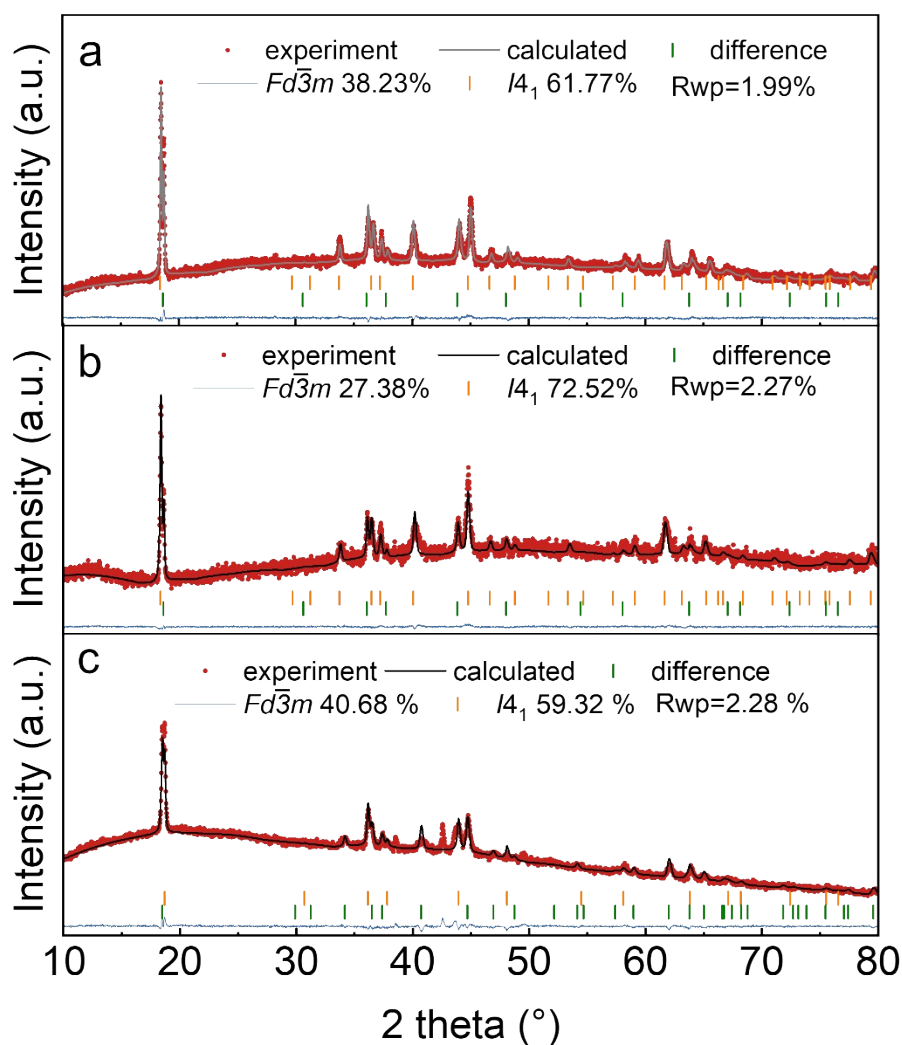


Fig. S4 (a) Ex situ XRD and Rietveld refinement results of the 1D2.5 V; (b) Refinement result of the 13D2.5 V; (c) Refinement result of the 26D2.5 V state.